RESEARCH ARTICLE

Preliminary Investigation of Fracture Behavior during Carbon Dioxide Fracturing of Natural Hydrogen Reservoir with Hard-Core Imperfections

Muhammad Usman Tahir[1] **and Shenglan Guo**[2,*]

[1] Atland Petro FZC, Sharjah 1377, United Arab Emirates
[2] Guangzhou Gas Group Co., Ltd., Guangzhou 511436, China

Abstract

The low concentration and poor reservoir properties of natural hydrogen suggest that reservoir stimulation measures such as fracturing is required for its efficient development. Nevertheless, the presence of reservoir imperfections, including hard and soft cores, can significantly affect fracture behavior during the fracturing operations. Moreover, there is currently a lack of relevant simulation and experimental studies addressing these effects. In the present work, the effects and mechanisms of hard cores on fracture propagation in natural hydrogen reservoirs in the Songliao basin were numerically simulated. In addition, various factors affecting propagation behavior of fracture were also analyzed. The investigation results indicate that the presence of hard cores induces the fracture propagation mode from "straight-line dominated" to "path optimization" (obstacle-avoidance) pattern, which consequently decreases propagation efficiency. The final fracture length exhibits a reduction of 12.63% compared with that in the homogeneous reservoir case, accompanied by an increase of 18.49% in the final fracture width. Furthermore, higher hard core strength and leakage coefficients significantly decrease fracture propagation efficiency, promoting the development of wide, short fractures. This research offers a preliminary theoretical framework to support the stimulation and efficient development of imperfection-bearing natural hydrogen reservoirs.

Keywords: natural hydrogen, carbon dioxide-based fracturing, reservoir imperfection, fracture initiation, fracture propagation.

1 Introduction

At present, fossil fuels such as coal, oil, and natural gas continue to play an important role in social and economic development. However, their unsustainable nature has made the pursuit of clean energy a priority on the global agenda [1]. The worldwide transition toward low-carbon and sustainable energy sources has highlighted hydrogen (H2) as a promising zero-emission clean energy carrier. According to

Submitted: 15 November 2025
Accepted: 10 January 2026
Published: 18 January 2026

Vol. 2, **No.** 1, 2026.
10.62762/RS.2025.759326

***Corresponding author:**
✉ Shenglan Guo
guosl2019@163.com

Citation
Tahir, M. U., & Guo, S. (2026). Preliminary Investigation of Fracture Behavior during Carbon Dioxide Fracturing of Natural Hydrogen Reservoir with Hard-Core Imperfections. *Reservoir Science*, 2(1), 34–51.

production methods and the corresponding carbon emission profiles, hydrogen energy is generally categorized into gray, blue, green, white, and red hydrogen. Blue hydrogen and gray hydrogen, both derived from fossil fuel reforming or gasification, currently serve as the primary sources of hydrogen supply. Green hydrogen is generated through electrolysis of water powered by renewable energy sources, such as wind and solar, making it the most environmentally sustainable form of hydrogen energy [2, 3]. Obviously, the above-mentioned forms of hydrogen are all artificially produced, and their production generates greenhouse gases, restricting the expansion of the hydrogen energy industry. The availability of naturally occurring hydrogen would offer greater economic efficiency and convenience. If hydrogen were available in a naturally occurring form, it would be both more economical and convenient [4]. This type of hydrogen,, commonly known as white hydrogen,, is generated through geological processes such as ultramafic rock serpentinization. It is distinguished by its abundance,, renewability, and minimal carbon footprint, highlighting its considerable development potential [5]. Up till now, natural hydrogen reservoirs characterized by high hydrogen concentrations have been discovered in numerous sedimentary basins around the world [6]. Recent exploration efforts in the Lorraine Basin (France) and the Mid-Continent Rift Valley (USA) has confirmed the presence of natural hydrogen with high concentrations (>90%) in reservoirs at depths of 1–3 kilometers. Such discoveries provide strong support for the further exploration and development of this resource.

However, the development of natural hydrogen reservoirs is challenged by geological complexities, including low permeability, pronounced heterogeneity, and the widespread occurrence of natural fractures [7, 8]. To enhance hydrogen recovery, hydraulic fracturing-a reservoir stimulation technology used in oil and gas reservoir-has been introduced to natural hydrogen reservoirs [9]. High-pressure fracturing fluid is injected to induce the initiation and propagation of fractures, thereby improving connectivity between the wellbore and the reservoir [10]. Unfortunately, reservoir imperfections, including hard cores, soft cores, and caves, may cause unpredictable propagation paths of fracture, complicating exploitation operations and reducing the fracturing effectiveness. Investigating the impact of these reservoir imperfections on fracture behavior optimizes stimulation design and enhances hydrogen recovery efficiency [11–13]. In addition, it can mitigate environmental risks, such as hydrogen leakage or groundwater contamination, while helping to maintain long-term reservoir integrity. Global natural hydrogen reserves are estimated at 5.6×106 million tons. This vast resource base provides significant development potential to support the achievement of net-zero carbon emissions by 2050 [14]. Therefore, this study aims to investigate how reservoir imperfections—such as hard cores and soft cores—regulate fracture behavior. The results are expected to provide a theoretical basis for the effective development of natural hydrogen reservoirs.

In recent years, investigations on natural hydrogen reservoirs have progressed rapidly. Initial studies mainly concentrated on exploration, resource assessment, and elucidation of generation mechanisms [15, 16]. These investigations have identified key geological processes responsible for hydrogen generation, such as serpentinization, as well as the necessary occurrence conditions, including impermeable cap-rocks and structural traps [17]. Natural hydrogen exhibits diverse origins and sources, and Table 1 presents the main geological origin of natural hydrogen. Hydraulic fracturing technology, developed through mature applications in the oil and gas industry, has been preliminarily applied to natural hydrogen reservoirs. For instance, Guo et al. [18] investigated the effects of various factors—including reservoir brittleness, and injection rate—on fracture propagation by developing a finite element model for simultaneous and zipper fracturing in hydrogen reservoir. The investigation findings reveal a notable difference in propagation behavior of fracture between the two fracturing strategies, with the propagation capacity of hydraulically-induced being slightly weaker for the case of simultaneous fracturing operations. Liang et al. [19] investigated the damage, as well as the application, of polymer fracturing fluid on natural hydrogen in tight hydrogen reservoirs through experimental studies. It was found that during reservoir stimulation using polymer fracturing fluid, nanoscale pores or throats are more susceptible to blockage by small particles from the rock matrix or fracturing fluid. Moreover, polymers can attach to pore surfaces, decreasing the effective pore size and consequently reducing the permeability. Liu et al. [20] numerically analyzed the reorientation and propagation behavior of fractures during the stimulation of low-permeability hydrogen reservoirs

Table 1. The main geological origin of natural hydrogen.

Classification of geological origin		Main mechanism
Organic	Thermal decomposition	Methylation, aromatization, and condensation of alkanes
	Microorganism	Fermentation of microorganisms and catalysis of biological enzymes
Inorganic	Escapes from Earth's core and mantle	Early retained hydrogen undergoes degassing and leakage through faults
	Reaction between water and reductant in mantle	Water in deep earth reacts with reduced metal ions in the mantle
	Serpentinization	Iron-rich rocks undergo redox reactions with water
	Fault activation	Reaction of silicate minerals with water
	Ionizing radiation	Water ionization by radioactive elements, and cracking of organic compounds caused by radiation
	Magma degassing	Volcanic gases containing hydrogen sulfide decompose at high temperatures

using radial holes-guided fracturing operation. The findings demonstrate that this technology allows better control over the directional propagation of hydraulically induced fractures, thereby enhancing recovery efficiency compared with conventional fracturing strategies. Lu et al. [21] investigated the impact of completion strategies on simultaneous fracture propagation in the development of natural hydrogen reservoirs by introducing a fracture propagation uniform index. The findings indicate that engineering strategies, such as reducing the number or diameter of perforations, as well as decreasing the number of outer cluster perforations, can optimize the geometry of hydraulically-induced fractures. Although these studies offer valuable insights, research on hydraulic fracturing in natural hydrogen reservoirs and the associated fracture behavior is still at an early stage and faces significant limitations [22]. The primary limitation arises from the absence of comprehensive studies on the effects of reservoir imperfections—such as hard cores, soft cores, and cavities—on fracture behavior, an area that remains largely unexplored to date. It is worth noting that hard cores, such as high-stiffness quartz, may cause fracture deflection or termination, whereas soft cores, such as clay fillings, may induce local stress concentration or fracture closure in fracturing operations [23, 24]. Furthermore, cavities—such as dissolution chambers—can cause fluid leakage or pressure anomalies, but their mechanisms in natural hydrogen reservoirs have not been comprehensively examined. Another limitation is that nearly all current research concentrates on water-based fracturing, which can result in problems such as Jamin's effect and water-sensitivity–induced reservoir damage. Fortunately, the anhydrous nature of CO_2-based fracturing fluid can effectively mitigate these issues. In addition, the use of CO_2-based fracturing fluid facilitates the formation of complex fracture networks in hydrogen reservoirs, which is beneficial for maintaining the sustained and stable production of natural hydrogen. In summary, the above-mentioned limitations constrain the advancement of hydraulic fracturing technology, highlighting the urgent need for targeted investigations into hard cores, soft cores, and cavities.

This article seeks to provide a preliminary examination of the influence of reservoir imperfections—such as hard cores—on fracture behavior during the stimulation of natural hydrogen reservoirs. To achieve this objective, this study consists of the following three parts.

1. A coupled fluid–solid mathematical model was developed as the basis for simulating fracture initiation and propagation in natural hydrogen reservoirs.
2. During the fracturing stimulation, the differences in the propagation behavior of fracture for case of hard cores were comparatively analyzed.
3. The influence of different factors on fracture behavior in hydrogen reservoirs with hard-cores was investigated.

The organization of this paper is as follows. Section 2 presents an overview of the study area, i.e., the hydrogen reservoirs in the Songliao Basin, covering geological settings and exploration history. Section 3 presents the mathematical model for simulating fracture initiation and propagation, including the

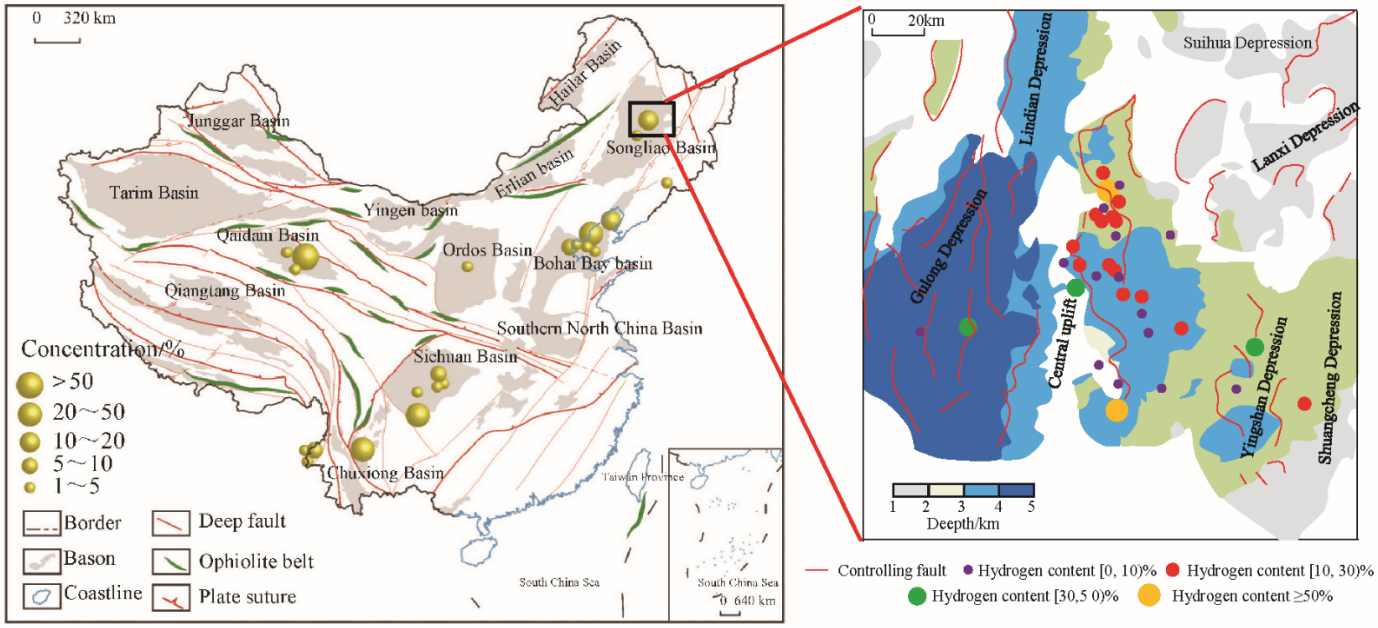

Figure 1. Distribution of natural hydrogen reservoirs within China and study area (Modified by Ref. [25]).

governing equations, boundary conditions, initial conditions, and applied loads. Section 4 provides a detailed analysis of the characteristics of fracture initiation and propagation in the presence of hard-core reservoir imperfections. Section 5 examines the influence of various factors on fracture behavior through sensitivity analysis. Finally, Section 6 concludes the paper by summarizing the key findings and proposing avenues for further investigation.

2 Study Area

Given its considerable potential for natural hydrogen generation and accumulation, China urgently requires advances in both geological research and the development of technologies for natural hydrogen reservoirs [25]. In China, multi-stage serpentinite—an important natural hydrogen source—is found at plate suture zones. Furthermore, a large number of active regional faults provide favorable pathways for the migration of natural hydrogen [26]. Figure 1 illustrates the distribution of natural hydrogen reservoirs in China, along with a geological overview of the study area.

As can be seen in Figure 1, the focus of this study, the Songliao Basin in northeastern China, is a large-scale rift basin trending NE–NNE, spanning an area of approximately 260,000 km^2 [25]. The basin, characterized by a complex structural framework, is situated at the convergence of the Mongol–Okhotsk, Paleo-Asian, and Pacific tectonic domains. Moreover, the basin exhibits a dual-layered architecture, consisting of an underlying fault depression and an overlying depression. The fault–depression sequence beneath the study area consists of the Huoshiling, Shahezi, Yingcheng, and Denglouku formations belonging to the Lower Cretaceous. Furthermore, gas accumulations occur in the source rocks of the Shahezi Formation, which are predominantly composed of glutenite. However, the overlying depression hosts the development of the Quantou, Qingshankou, Yaojia, Nenjiang, Sifangtai, and Mingshui formations. Within the primary source rocks surrounding the Qingshankou Formation, which are dominated by sandstone, three separate petroleum systems are documented. The presence of hydrogen is evidenced by results from multiple exploration wells in the northern sector of the basin, and hydrogen-rich natural gas is generally occurs within the central uplift. Quantitative statistical analysis demonstrates that the hydrogen concentrations in natural gas samples in the northern Songliao Basin vary between 1.00% and 85.54%, with a mean value of 9.88%, indicating considerable resource potential. Among the mixed gas components, nitrogen accounts for the highest proportion, with an average content exceeding 20%, while carbon dioxide represents the lowest proportion, with an average content below 5%.

The SK-2 well is located within the Xujiaweizi fault depression in the central depression of the Songliao Basin. It represents the deepest scientific exploration well drilled since the inception of the International Continental Scientific Drilling Program (ICDP). For

this exploration well, distinct hydrogen anomalies were detected within the sandstone section of the Denglouku Formation, with burial depths ranging from approximately 2,540–2,965 m in the upper part and 2,965–3,082.8 m in the lower part. However, these reservoirs show relatively poor physical properties, and the pore sizes of the samples are mainly distributed between 3 and 12 nm, corresponding to mesoporous structures [25]. In this context, reservoir stimulation measures, such as fracturing operation, are essential for the efficient development of natural hydrogen resources in the region.

3 Mathematical model for fracture initiation and propagation in hydrogen reservoirs

3.1 Modeling Assumptions

To facilitate modeling and numerical computation, the following key assumptions were employed in this study. (1) The reservoir matrix is assumed to be homogeneous and isotropic, with identical properties at all locations within the model. (2) The properties of the fracturing fluid (such as the compressibility, density and viscosity) are assumed to remain constant throughout the fracturing process and are not affected by factors such as temperature variations. (3) Physical and chemical interactions between the reservoir fluids and the fracturing fluid, including mixing and dissolution, are neglected. (4) Fracturing fluid flow is a one-dimensional laminar flow along the length direction of fractures. (5) The reservoir matrix rock and hard cores are assumed to behave as elastic media, with plastic deformation neglected. Based on these assumptions outlined above, the mathematical model was formulated.

3.2 Governing Equations of The Mathematical Model

3.2.1 Stress equilibrium equation and continuity equation

The stress equilibrium equation governing the fracturing process in natural hydrogen reservoirs can be expressed as follows [27]:

$$\begin{cases} \dfrac{\partial \sigma_{xx}}{\partial x} + \dfrac{\partial \sigma_{yx}}{\partial y} + \dfrac{\partial \sigma_{zx}}{\partial z} - \alpha \dfrac{\partial p}{\partial x} + f_x = 0, \\ \dfrac{\partial \sigma_{xy}}{\partial x} + \dfrac{\partial \sigma_{yy}}{\partial y} + \dfrac{\partial \sigma_{zy}}{\partial z} - \alpha \dfrac{\partial p}{\partial y} + f_y = 0, \\ \dfrac{\partial \sigma_{xz}}{\partial x} + \dfrac{\partial \sigma_{yz}}{\partial y} + \dfrac{\partial \sigma_{zz}}{\partial z} - \alpha \dfrac{\partial p}{\partial z} + f_z = 0, \end{cases} \tag{1}$$

where σ_{xx}, σ_{xy}, σ_{xz}, σ_{yy}, σ_{yz} and σ_{zz} are six components of geostress, p is the pore pressure, α is the Biot's coefficient, f_x, f_y and f_z are three components of body force.

Equation (1) can be expressed in tensor form, as shown in Equation (2):

$$\nabla \cdot (\mathbf{D} : \boldsymbol{\varepsilon}) - \alpha \nabla p + \mathbf{f} = 0 \tag{2}$$

where $\mathbf{D}$ is the elastic stiffness matrix, $\boldsymbol{\varepsilon}$ is the strain tensor, $\mathbf{f}$ is the body force tensor.

By substituting Darcy's law into the mass balance equation, the final tensor form of the continuity equation can be obtained, as follows:

$$\nabla \cdot [\mathbf{K} \cdot (\nabla p - \rho_f \mathbf{g})] + Q_s = 0 \tag{3}$$

where $\mathbf{K}$ is the absolute permeability, ρ_f is the fluid density, $\mathbf{g}$ is the gravitational acceleration, Q_s is the fluid injection rate.

The fracture flow equation employed in this study is a key component of the mathematical model for propagation of fractures based on the extended finite element method (XFEM) [28]. It establishes a strong coupling between the hydraulic field inside the fracture and the mechanical opening of the fracture walls (i.e., the fracture width, w), and it can be written as:

$$\nabla \cdot \left[\frac{w^2}{12\mu} \mathbf{t} \cdot (\nabla p - \rho_f \mathbf{g}) \right] + Q_{f,\text{source}} = 0 \tag{4}$$

where w is the fracture width, $\mathbf{t}$ is a second-order tensor that projects the pressure gradient ∇p onto the tangential direction of the fracture, $Q_{f,\text{source}}$ denotes the rate at which fracturing fluid leaks from the fracture into the surrounding reservoir.

3.3 Criteria for initiation and propagation of fracture

Fracture initiation occurs once the stress or strain satisfies the defined initiation criterion. At present, several commonly used criteria are available for determining fracture initiation in finite element simulations [29, 30]. Among them, the maximum principal stress criterion, maximum principal strain criterion, maximum normal stress criterion, and maximum normal strain criterion are the most widely adopted [31]. Owing to its high numerical stability and favorable convergence performance, the maximum principal stress criterion is adopted in this study. The

maximum principal stress criterion can be expressed as:

$$f = \left\{ \frac{\sigma_{\max}}{\sigma_{\max}^{d}} \right\} \tag{5}$$

where $\sigma_{\max}^{d}$ is the critical value of the maximum principal stress experienced by the investigation element. An element is considered to be damaged and a crack is initiated only when the maximum stress ratio reaches its critical value, that is, when the parameter f in Equation (5) is greater than or equal to 1.0.

For effective reservoir stimulation, fractures need to propagate after initiation. Once fracture initiates, the damage value can be determined using fracture energy theory. In this study, fracture propagation is evaluated according to the B–K criterion [32]. The fracture energy can be calculated using the following formula:

$$G_n + (G_s - G_n)\left(\frac{G_s}{G_t}\right)^{\eta} = G_c \tag{6}$$

where η is the material constant, G_n is the normal fracture energy, G_s is the first tangential fracture energy, G_t is the second tangential fracture energy. G_c represents the area enclosed by the coordinate axes beneath the traction–separation (T–S) softening curve.

When

$$\frac{G_t}{G_c} \geq 1 \tag{7}$$

fracture propagation occurred.

The direction of fracture propagation is governed by the Maximum Tangential Stress (MTS) criterion, which indicates that the fracture propagates along the direction where the circumferential stress reaches its maximum value.

In polar coordinates (r, θ), the stress field near the fracture tip is expressed as:

$$\begin{aligned} \sigma_\theta = {} & \frac{K_I}{\sqrt{2\pi r}} \cos\frac{\theta}{2}\left(1 - \sin\frac{\theta}{2}\sin\frac{3\theta}{2}\right) \\ & + \frac{K_{II}}{\sqrt{2\pi r}} \sin\frac{\theta}{2}\cos\frac{\theta}{2}\cos\frac{3\theta}{2} \end{aligned} \tag{8}$$

where σ_θ is the circumferential stress, K_I and K_{II} are the stress intensity factors in two modes. According to the MTS criterion, the propagation angle of the fracture satisfies the following relationship:

$$\frac{\partial \sigma_\theta}{\partial \theta} = 0 \tag{9}$$

3.4 Loads, initial and boundary conditions

The mathematical model incorporates two primary physical fields, namely the mechanical and hydraulic fields, and appropriate boundary and initial conditions should be applied independently for each field [33]. At the beginning of the simulation $(t = 0)$, the reservoir is considered to be in a state of initial stress equilibrium. This equilibrium state can be expressed as follows:

$$\sigma_{ij}(x, y, z, t = 0) = \sigma_{ij}^{0} \tag{10}$$

where σ_{ij}^{0} is the initial stress tensor, which usually includes the minimum and maximum horizontal principal stresses and vertical principal stresses.

Similarly, the pore pressure within the entire reservoir domain is considered to be in hydrostatic equilibrium, represented by the following relationship:

$$p_0(x, y, z, t = 0) = p_0^{0} \tag{11}$$

where p_0^{0} is the initial pore pressure, which is usually related to depth.

In this study, the mechanical boundary conditions refer to displacement-constrained boundaries, which can be expressed as Equation (12):

$$U_n = 0 \tag{12}$$

where U_n is the normal displacement of model boundaries.

For the pressure boundary condition, a constant initial pore pressure is applied to the outer boundary of the model, which can be expressed in the form of Equation (13):

$$p_0 = p_0^{0} \tag{13}$$

The injecting load is applied as a flow source term at the initiation point of the fracture, as expressed below:

$$Q_s(x, y, z, t) = Q_{\text{inj}}(t) \tag{14}$$

where $Q_{\text{inj}}(t)$ is the injection rate of fracturing fluid that varies over time.

4 Fracture Behavior Under Various Reservoir Imperfections

4.1 Geometric Model

As is well known, reservoir properties, including reservoir strength and in-situ stress, directly influence the fracture initiation pressure, propagation path,

and final fracture geometry [28]. Among these factors, reservoir imperfections, as a form of geological heterogeneity, can markedly disturb fracture behavior, potentially causing fracture reorientation, branching, or even termination of propagation. Therefore, the presence of reservoir imperfections increases the complexity of fractures, thereby affecting oil and gas production [34, 35].

In the present work, the case of hard core, was investigated, and the geometric models were presented in Figure 2. As shown in Figure 2(a), the homogeneous model is a regular square with both length and width of 100 m, and the injection point is located at the midpoint of the lower boundary of the model. This case of a homogeneous reservoir is designed to serve as a baseline for comparison with models that include reservoir imperfections. As illustrated in Figure 2(b), the hard-core case differs from the homogeneous model (Figure 2(a)) only by the inclusion of a hard-core distribution region with dimensions of 6.0 × 6.0 meters. Within the hard-core distribution region, hard cores measuring 1.0 meter in length and width are uniformly distributed at regular intervals, and each pair of adjacent hard cores is separated by a 1.0 m × 1.0 m reservoir rock. In this case, the injection point remains located at the center of the bottom boundary of the model, and the distance between the bottom boundary of the hard-core distribution area and the model bottom boundary is 27 m. For convenience, the two subgraphs in Figure 2 correspond to the study conditions referred to as Case 1 and Case 2, respectively.

In fact, it is relatively simple to switch between the simulation configurations of the two cases shown in Figure 2. In the simulation, only the properties of the sediments within the hard-core or soft-core regions need to be modified. Both two models consist of 10,000 CPE4P elements, which are used to simulate the initiation and propagation of fractures during the fracturing process. Furthermore, only one analysis step of the Soils type was defined in the simulation, and the total simulation time was set to 500 s. In addition, the boundary conditions, initial conditions, and loads of the two geometric models are summarized in Table 2.

4.2 Basic Simulation Parameters

To date, exploration on natural hydrogen reservoirs in the Songliao Basin primarily focuses on their depth and hydrogen content, whereas studies on the mechanical properties remain limited [36, 37]. Therefore, the parameters used in the fracturing simulations of this study are derived from previous simulation studies of fracturing operation in oil and gas reservoirs within this basin. The basic simulation data for fracturing in natural hydrogen reservoir are summarized in Table 3.

4.3 Grid Independence Analyses

The primary objective of numerical research is to achieve simulations that are both accurate and efficient. Therefore, grid independence analysis is crucial [38]. To evaluate the grid independence, the homogeneous model shown in Figure 2(a) was used to analyze fracture propagation with element sizes of 0.5 m, 1.0 m, and 1.5 m respectively. The analysis results were presented in Figure 3. In addition, similar analyses were performed for another one model illustrated in Figure 2 to ensure consistency.

Although Figure 3(a) presents the final fracture morphologies under three different grid sizes, qualitative comparison of fracture morphology alone is insufficient to assess grid independence. From Figures 3(b–d), it can be observed that as the grid size increases, the total initiation pressure decreases, the initiation-point fracture width is reduced, and the overall simulation time becomes shorter.. Nevertheless, the relationships between grid size and these parameters are nonlinear, indicating that mesh refinement does not lead to proportionally consistent changes. As shown in Figure 3(b), when the grid size increases from 0.5 m to 1.0 m, both the initiation pressure and the propagation pressure change slightly. Specifically, the initiation pressure decreases from 99.57 MPa to 97.28 MPa, while the propagation pressure drops from 60.50 MPa to 59.29

Table 2. The boundary conditions, initial conditions, and loads.

	Type	Objection	Value
Boundary conditions	Displacement Pore pressure	Outer boundaries	Normal displacement is 0 Initial pore pressure
Initial conditions	Pore pressure Stress	Whole model	Initial pore pressure In-situ stresses (σH, σh, and σV)
Loads	Injection rate	Injection node	Injection rate of fracturing fluid

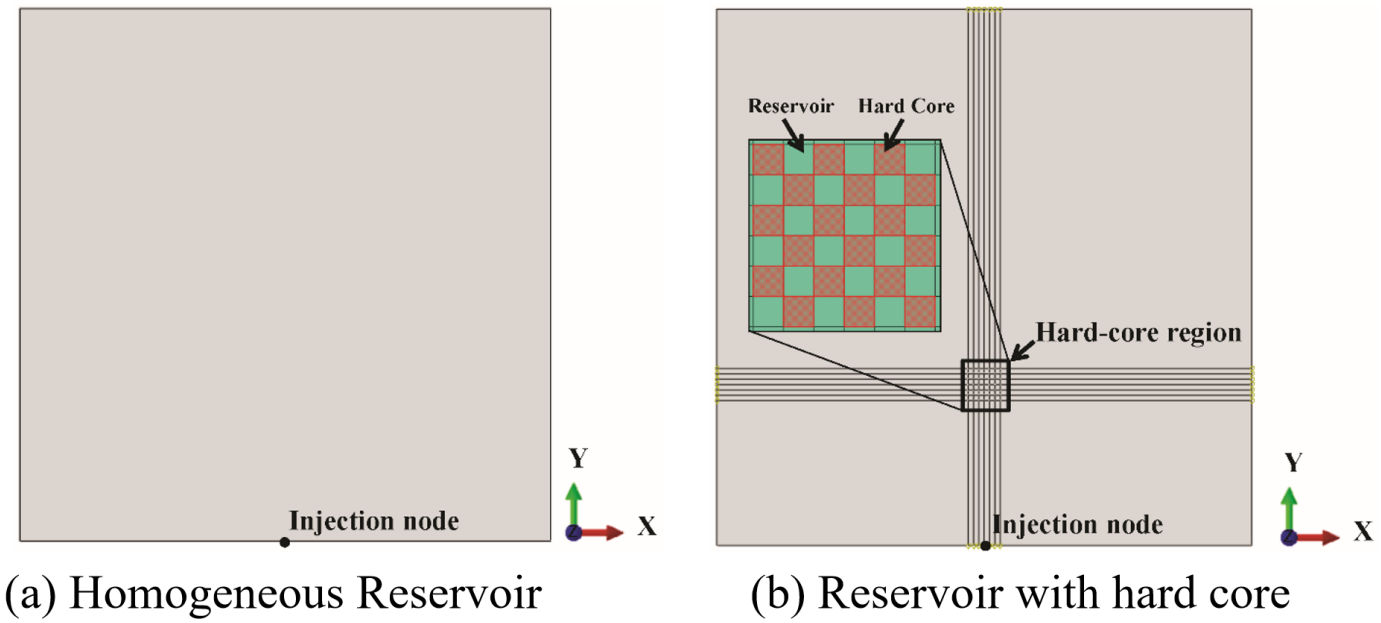

Figure 2. Geometric model for investigating effect of fracture reorientation on fracture behavior.

MPa. In contrast, increasing the grid size from 1.0 m to 1.5 m led to a marked reduction in both initiation and propagation pressures. The fracture width at the injection point, as shown in Figure 3(c), exhibits a similar trend with respect to grid size. The variation in fracture width is negligible within the grid size range of 0.5 m to 1.0 m, but becomes significant when the grid size increases from 1.0 m to 1.5 m. In this case, further reducing the grid size beyond 1.0 m (i.e., increasing the number of elements) does not lead to a meaningful improvement in the accuracy of the simulation results.

However, as the grid size increases, the total number

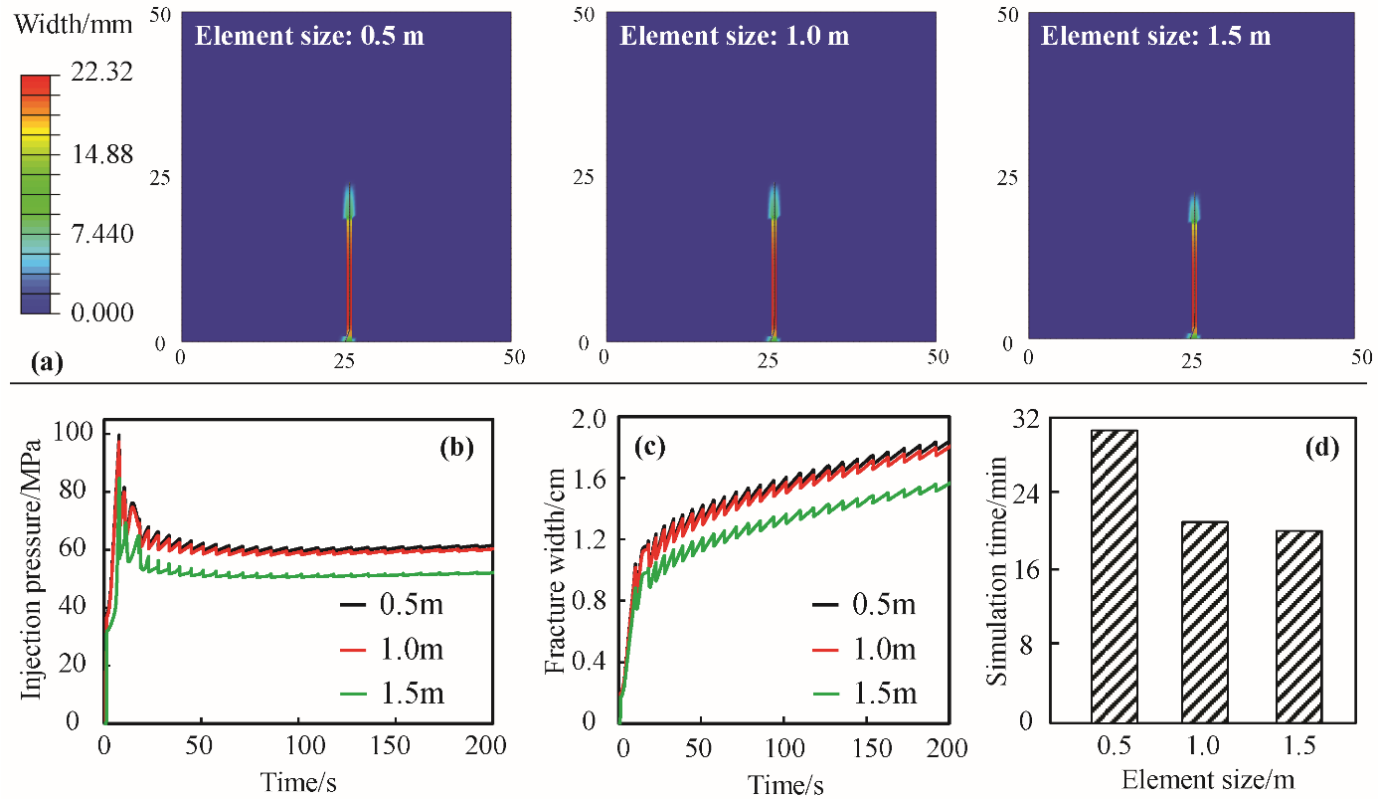

Figure 3. Grid independence analyses results (the simulation time of 200s). (a) The final fracture morphology; (b) Injection pressure; (c) Fracture width; (d) Simulation time.

Table 3. The basic simulation data (default case).

Object	Parameters	Value	Unit
Reservoir	Elastic Modulus	20	GPa
	Poisson ratio	0.25	-
	Initial void ratio	0.15	-
	Initial permeability	0.1	$10^{-3}\mu m^2$
	Tensile strength	5.0	MPa
	Leakoff coefficient	10^{-14}	m/(mPa·s)
	Pore pressure	15	MPa
	In-situ stresses	σ_H=15, σh=18 and σV=16	MPa
Hard core	Elastic Modulus	40	GPa
	Poisson ratio	0.20	-
	Initial void ratio	0.15	-
	Leakoff coefficient	10^{-14}	m/(mPa·s)
	Initial permeability	0.01	10^{-3} μm^2
	Tensile strength	10.0	MPa
CO_2-Based fracturing fluid	Fluid viscosity	5.0	mPa·s
	Injection rate	10	m^3/min
Perforation	Length	0.75	m
	Azimuth	30	°

of elements in the model gradually decreases, and the simulation time is markedly reduced when the grid size increases from 0.5 m to 1.0 m (see Figure 3(d)). Within the range of 1.0 m to 1.5 m, increasing the grid size leads to only a limited decrease in simulation time. In other words, simulation efficiency has not been enhanced by decreasing the number of elements within a grid size larger than 1.0 m. Therefore, taking both simulation accuracy and computational efficiency into account, a grid size of 1.0 m is considered appropriate.

4.4 Fracture Behavior Under Various Types of Reservoir Imperfections

Based on the above model, the evolution of parameters such as injection pressure, fracture width, and fracture morphology in fracturing was analyzed. Figure 4 presents both qualitative and quantitative comparisons of fracture behavior between Case 1 and Case 2 during fracturing operation. As shown in the qualitative comparison in Figure 4(a), the presence of hard cores leads to a significant difference in fracture geometry compared with the homogeneous reservoir. In the homogeneous reservoir, the 30° perforation leads to a slight deflection, after which the fracture extends nearly straight along the Y-direction. However, when hard cores are present, the fracture initially propagates along the Y-direction and then undergoes deflection and reorientation within the hard core distribution region. During this process, the fracture deviation occurred at 295.4 seconds after the start of the fracturing operation. After deflection, the fracture is reoriented toward its original linear propagation path after 165.8 seconds of propagation. It can be inferred that if the fracturing simulation continues, the fracture propagation path would realign with the Y-direction and continue to extend along a straight trajectory. Finally, the fracture exhibits a slightly arcuate configuration within the hard core distribution region. Obviously, the presence of hard cores transforms the fracture propagation mode from a 'straight-line dominated' pattern to a 'path-optimization' (obstacle-avoidance) behavior, thereby reducing propagation efficiency. This phenomenon is common in unconventional geo-energy development, where hard cores act as 'barriers' that influence the fracturing performance [39]. Nonetheless, since the strength of hard cores in this case was not significantly different from those of the surrounding reservoir, the fractures did not completely bypass the hard-cores but propagated through them by the arcuate shape [40].

The differences in fracture morphology can be further quantified by analyzing the time-series curves of injection parameters, as well as key fracture characteristic parameters. As shown in Figure 4(b), there is essentially no difference in injection pressure between Case 1 and Case 2 before the fracture reaches the hard core distribution region. For both cases, the initiation pressures (87.98 MPa and 87.87 MPa) and initiation times (7.74 s and 9.11 s) are almost

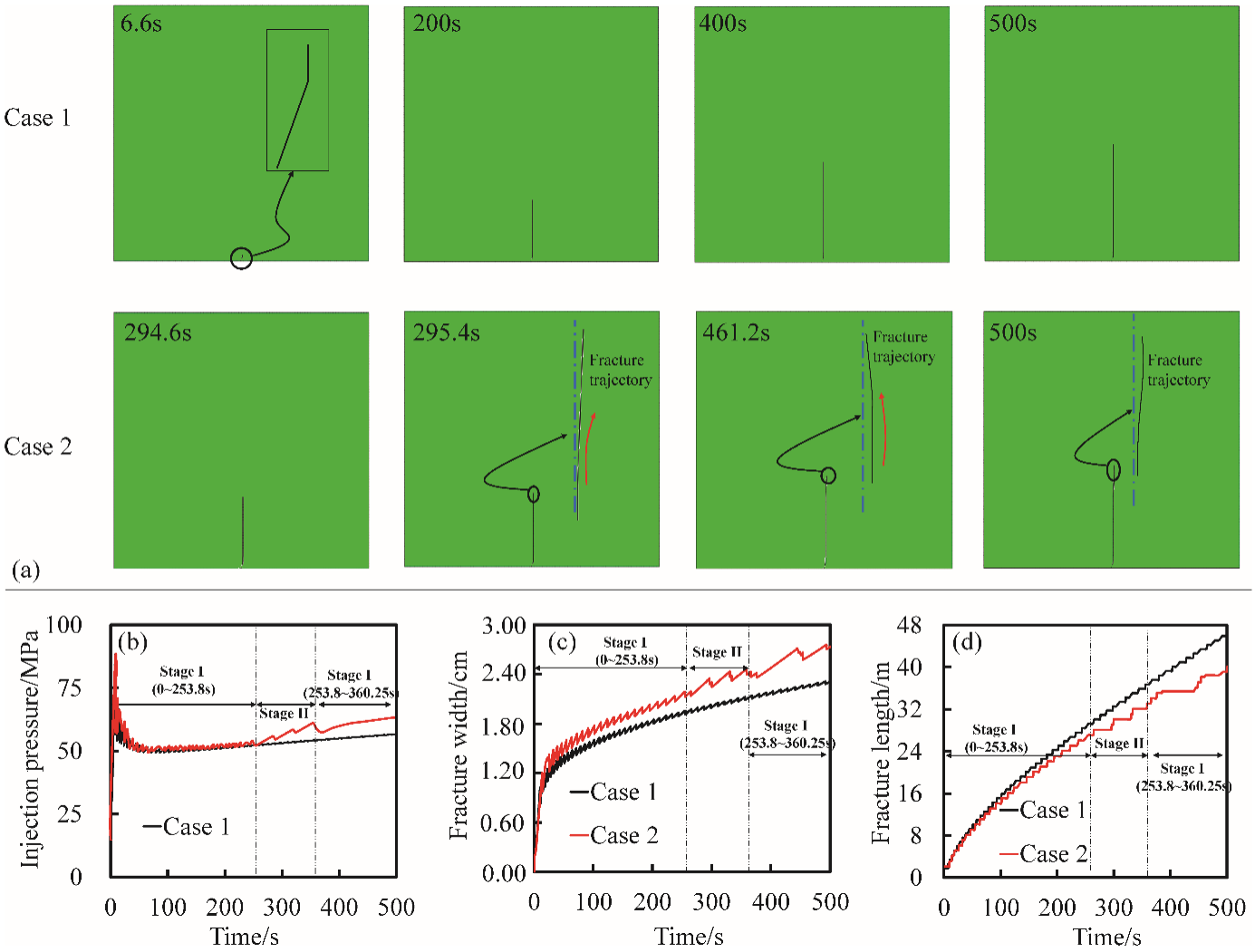

Figure 4. Comparison of fracture behavior between Case 1 and Case 2. (a) Fracture geometry, (b) Injection pressure, (c) Fracture width, (d) Fracture length.

the same, indicating negligible differences in fracture initiation behavior. This is because, in both cases, the fractures are initiated within the same sediment, which is homogeneous reservoir. However, in the later stage of fracturing, the evolution characteristics of the injection pressure differ between the two cases. In Case 1, the injection pressure exhibits a steady decline followed by stabilization, ultimately maintaining a fracture propagation pressure of 56.52 MPa. However, in the presence of hard cores within the reservoir, the evolution of injection pressure can be divided into three stages (i.e. I, II and III stages in Figure 4(b, c)). Specifically, the three stages are divided by two time nodes, 253.8 s and 360.25 s, corresponding to the time when the first hard core is encountered and the third hard core was propagated past, respectively. For Case 2, an obvious fluctuation in the injection pressure was observed during the later stage of fracturing. The pressure fluctuations observed in Stage II are attributed to the increased injection pressure required each time the fracture propagates through a hard core element. The pressure fluctuations observed in Stage III arise from the additional resistance that must be overcome during the reorientation of the fracture back toward the Y-direction.

In addition, the presence of hard cores in the reservoir can significantly affect both fracture width and fracture length. For the homogeneous reservoir, it can be seen that the fracture width at the injection node increases steadily throughout the fracturing operation, although the rate of widening gradually decreases (see Figure 4(c)). Furthermore, the fracture length also increases gradually and smoothly (see Figure 4(d)), and the final fracture width at the injection node and the total fracture length are 2.3 cm and 45.94 m, respectively. Overall, all these evolution trends of fracture width and length in homogeneous reservoirs are consistent with those reported in previous studies. For Case 2, a steady increase in fracture width at

the injection node is observed during the initial stage, accompanied by smooth fracture propagation. Although the sediments through which the fracture propagates during this stage are similar to those in Case 1, the fracture width at any given time is longer, whereas the fracture propagation rate is slower. This behavior arises because, although the fracture does not intersect the hard core during the initial stage, the presence of the hard core has already altered the stress distribution throughout the model. By the end of the first stage, the fracture at the injection point had widened to 2.19 cm, and the total fracture length had extended to 26.13 m. In the second stage, when the fracture tip encounters each hard core, fracture propagation pauses for 30.00 s, 29.54 s, and 25.37 s, respectively. Throughout this period, the fracturing fluid was continuously injected into the reservoir. The continuous injection of fluid into a nearly constant fracture volume inevitably results in fracture to exhibit oscillatory widening. Figure 5 shows the mechanism of this process. By the end of the second stage, the width of the fracture at the injection node had increased to 2.42 cm, while the total fracture length extended to only 32.13 m. The fracture propagation rate during the second stage is markedly reduced compared with that in the first stage, owing to the need to traverse three hard cores. At the onset of the third stage, the fracture has penetrated the hard cores and extends into the homogeneous reservoir. At this stage, the fracture tip no longer propagates strictly along the Y-direction but instead exhibits an inclined trajectory. During Stage III, the fracture undergoes two reorientations in its propagation direction. In both reorientation processes, the stress concentration at the fracture tip rises markedly, resulting in restricted propagation. Correspondingly, the fracture width at the injection point also experienced two rounds of widening, and mechanism was similar to that shown in Figure 5. Affected by the presence of hard cores and fracture reorientation throughout the entire fracturing process, the final fracture width in Case 2 is 18.49% greater than that in Case 1, whereas the final fracture length decreases by 12.63%.

In summary, the influence of hard cores on fracture propagation is evident in both the second and third stages, but the mechanisms in the two stages are different. In the second stage, the high tensile strength of the hard core directly delays fracture propagation by prolonging the time required for their tensile failure [41]. However, in the third stage, its impact is indirect. The stress concentration in the reservoir element around the fracture tip during the reorientation process will once again affect its effective propagation.

5 Factors Affecting Fracture Behavior During Fracturing in Reservoir with Hard Cores

A comprehensive exploration of the mechanisms and influence patterns of various factors affecting fracture behavior during fracturing is essential for improving the design and optimization of fracturing operations. Based on the basic simulation parameters listed in Table 1, the effects of factors such as strength of hard core, and differences between in-situ stresses on the fracture morphology were investigated. It is worth mentioning that all sensitivity analyses were performed by varying the corresponding investigation parameters listed in Table 3 while keeping all other parameters unchanged.

5.1 Effect of Hard-core Strength

The strength of the hard cores inevitably influences the behavior of fractures, where the strength specifically refers to the tensile strength. In this study, the fracture behavior was investigated for hard cores with tensile strengths of 7.5, 10.0, 12.5, and 15.0 MPa.

Figure 6 presents the evolution curves of fracture length and fracture width at the injection node for different tensile strength. As observed in Figure 6, an increase in the hard-core strength exerts a pronounced influence on fracture propagation. Specific analysis can be conducted based on the width and length of the fracture. At a hard core strength of 7.5 MPa—only 2.5 MPa higher than that of the homogeneous reservoir—the fracture still propagates through all three hard core elements, although along a deflected trajectory. The difference in fracture behavior between this case and the homogeneous reservoir is consistent with the statement provided in Section 4.4; therefore, it will not be discussed in further detail in this section. In this case, the final fracture length is 41.47 m, which is 4.47 m shorter than that observed under homogeneous reservoir conditions. This reduction of fracture length mainly results from the delayed propagation that occurs as the fracture propagates through three hard cores. At a hard core strength of 10.0 MPa, the evolution patterns of the fracture width curve at the injection node and fracture length curve closely resemble those observed at 7.5 MPa. The main difference between the two cases arises during the final stage of fracturing, when the fracture interacts with and propagated through the three hard

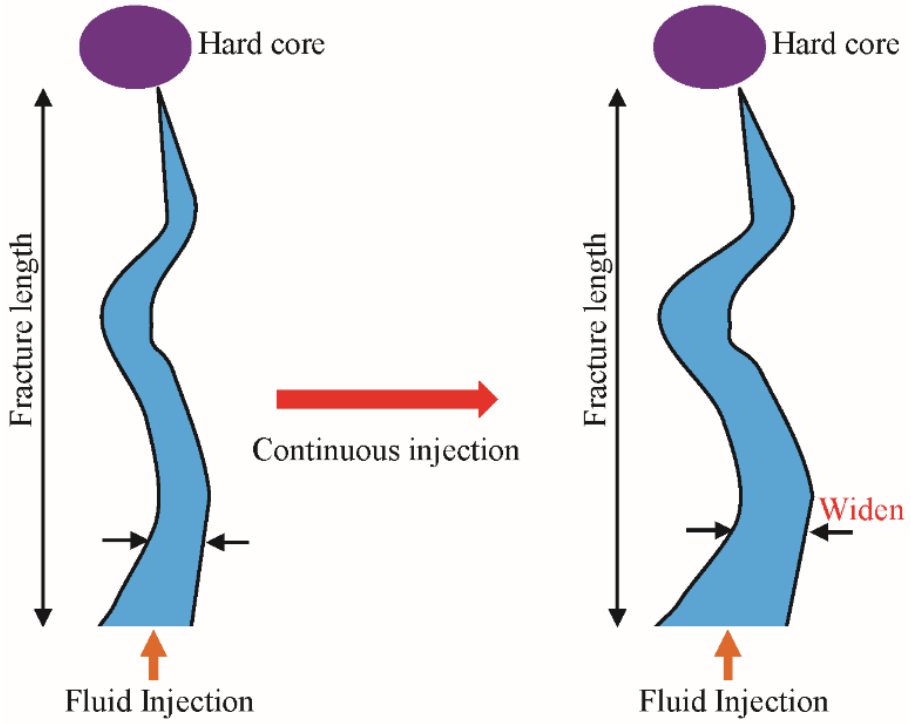

Figure 5. Mechanism of fracture widening at the injection point as the fracture tip interacts with a hard core.

cores [42]. Obviously, after penetrating the hard cores, the reorientation of the fracture at a tensile strength of 7.5 MPa is more favorable for subsequent fracture propagation (see Figure 6(b)). Under both hard core strength conditions, the fracture can still propagate smoothly through the hard cores and subsequently undergo reorientation and further propagation. The fracture propagates an additional 11.33 m and 10.00 m beyond the hard cores at strengths of 7.5 MPa and 10.0 MPa, respectively.

However, at a hard core strength of 12.5 MPa, the fracture propagation through the three hard cores is significantly hindered, and reorientation after propagating through three hard cores is extremely difficult. Therefore, the fracture propagation terminated almost immediately once it passed through the three hard core elements, resulting in the forced termination of the fracturing operation. By the end of the fracturing process, the total fracture length was 31.13 m, representing a reduction of 14.81 m compared with the homogeneous reservoir case. Moreover, the curves in Figure 6 indicate that the fracture requires a longer time to propagate through the three hard core elements compared with the two lower-strength cases (i.e., 7.5 MPa and 10.0 MPa). Moreover, the fracture width at the injection node increases rapidly as the fracture propagates through the three hard core elements. At the end of fracturing operation, the fracture width at the injection node was increased to 0.34cm. The mechanism of this can be explained by Figure 7. As presented in Figure 7, when the fracture tip is located within a hard core element with higher tensile strength, the fluids within this fracture element must overcome greater resistance for continue propagating. In this way, more working fluid must accumulate along the entire fracture to provide the necessary driving force for fracture propagation [43]. As a result, all elements of the fracture will inevitably widen and the propagation will naturally be delayed. It can also be seen from Figure 6 that the injection flow rate is no longer provide sufficient support to allow fracture to propagate within any hard core element when the strength of hard core increases as 15.0 MPa. Although a large volume of fluid continues to accumulate in the fracture, and the fracture width at the injection node keeps widening, yet it fails to drive further propagation within the first hard core. As the fracture width at the injection node widens to 3.8 cm, the fracture can no longer propagate, since the shear stress at the fracture tip fails to exceed the tensile strength. This thereby forces the simulation to end, which is 99.42 seconds earlier than the end time at a tensile strength of 12.5 MPa.

5.2 Effect of Filtration Coefficient

In general, drilling or fracturing operations conducted in denser reservoirs exhibit weaker filtration of working fluid due to the lower permeability of

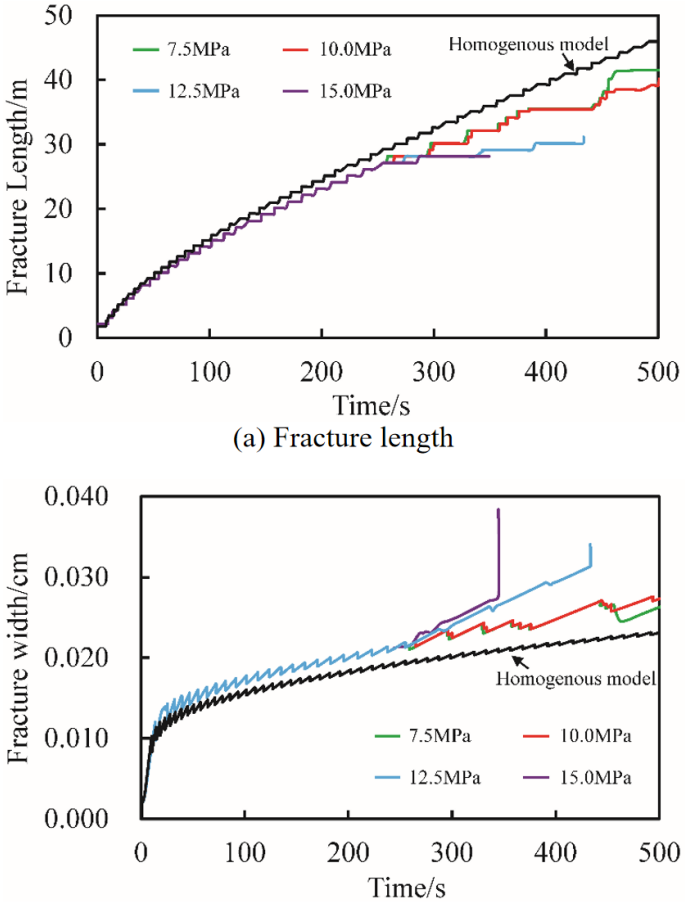

(a) Fracture length

(b) Fracture width at the injection node

Figure 6. The fracture behavior for different strength of hard cores.

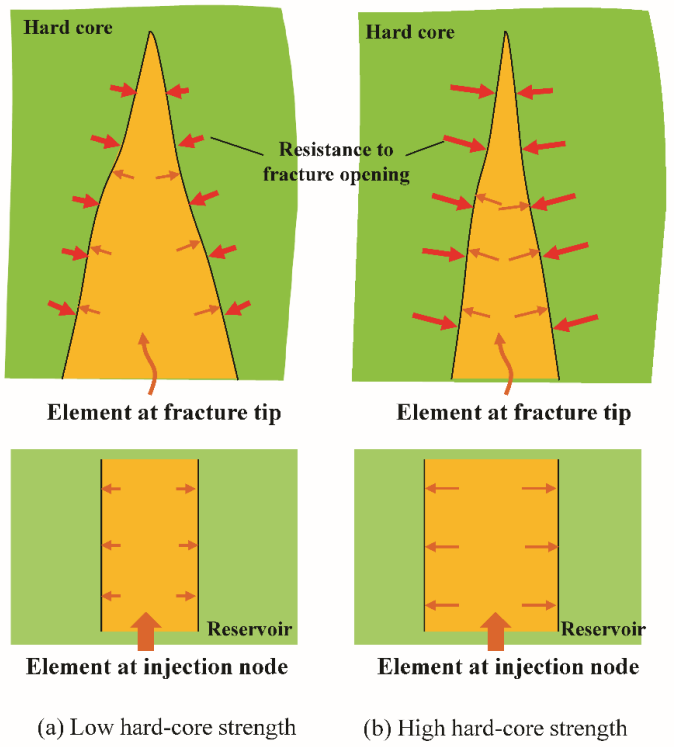

(a) Low hard-core strength (b) High hard-core strength

Figure 7. Schematic diagram of the influence mechanism of hard core on fracture propagation.

the reservoir matrix [44]. However, in loose sediments, the fracturing fluid tends to leak into the surrounding formation through the fracture walls, which consequently reduces the pressure accumulation within the fracture. In essence, hard cores refer to dense rock particles distributed within conventional reservoir sediments. Naturally, fracture within the hard core distribution section exhibit lower leakage coefficients on both fracture surfaces [45]. Therefore, the fracture propagation behavior was investigated under hard core leakage coefficients of 2.5×10^{-15}, 5.0×10^{-15}, 7.5×10^{-15}, and 1.0×10^{-14} m/(mPa·s), respectively.

Figure 8 presents the evolution curves of fracture length and fracture width at the injection node under different leakage coefficients. From Figure 8, it is clear that the leakage coefficient of within the hard core influences the fracture behavior during and after propagating through the hard core elements. That is, its effect is limited to the time interval Δt shown in Figure 8(a). As observed in Figure 8, as the leakage coefficient increases, the time for fracture propagates through each hard core element is prolonged during the process of fracture propagating through hard core elements. The time required for fracture to propagate through three hard cores under different leakage coefficients is quantitatively shown in Figure 9. Taking the first hard core as an example, the time required for the fracture to pass through the hard core element for the four leakage coefficients is 22.5 s, 25.35 s, 28.35 s, and 30.15 s, respectively. It is evident that a smaller leakage coefficient leads to faster fracture propagation within the hard core. A similar trend is observed for the other two hard core elements. The mechanism by which the leakage coefficient influences fracture propagation in this stage is illustrated in the schematic diagram shown in Figure 10. As can be seen in Figure 10, when the leakage coefficient is small, the fluid within the fracture only slightly infiltrates into the surrounding sediment through the two fracture walls (See Figure 10(a)). In this case, the pressure at the fracture tip must be sufficiently high to rapidly propagate the fracture. However, when the leakage coefficient is high, a significant amount of working fluid from the fracture leaks into the surrounding sediment, the lower pressure can't effectively propagate the fracture in hard core elements (See Figure 10(b)). However, it should be noted that when the leakage coefficient is as low as 2.5×10^{-15} m/(mPa·s), the fracture no longer exhibit

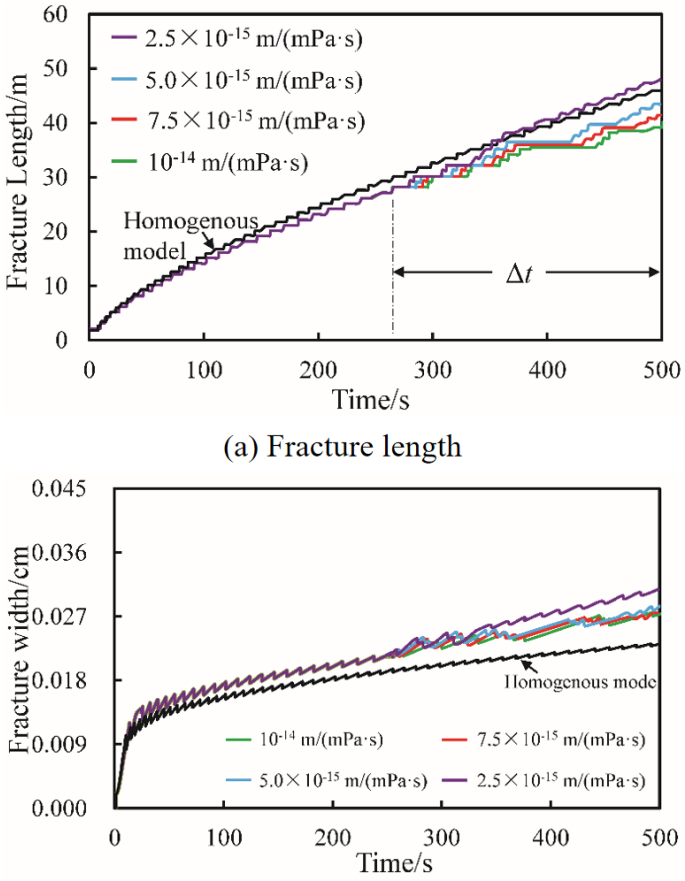

Figure 8. Effect of leakage coefficient on fracture propagation.

the "obstacle-avoidance" behavior but propagate directly through them. This occurs because the low leakage of the working fluid increases the pressure at the fracture tip, generating sufficient shear stress to overcome the tensile strength of the hard core and facilitate fracture propagation [46, 47].

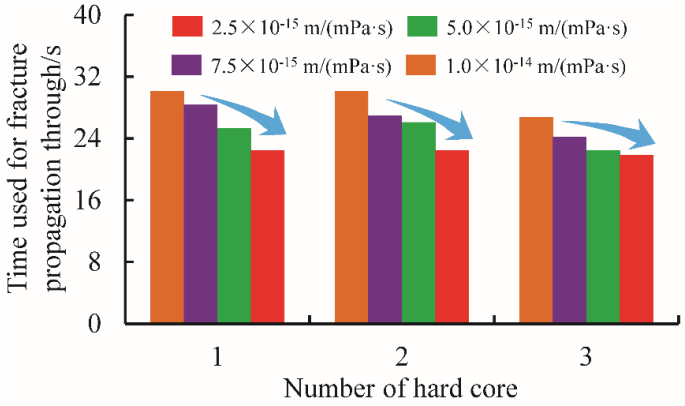

Figure 9. Comparison of the time taken for fracture propagating through three hard core elements under different leakage coefficients.

Even after the fracture has propagated through the three hard cores, its propagation behavior remains influenced by the leakage coefficient within the hard-core distribution region. However, because the hard-core section is only 3.0 m long—representing merely about 3% of the total model size—its overall influence on the fracture propagation behavior remains limited. Therefore, after the fracture propagates through three hard cores, the fracture widths at the injection node show aminor differences among the three leakage coefficients of 5.0×10^{-15}, 7.5×10^{-15}, and 1.0×10^{-14} m/(mPa·s). Nevertheless, notable differences remain in the final fracture lengths for these three leakage coefficients. The final fracture lengths obtained from the three simulations are 43.43 m, 40.86 m, and 39.82 m, respectively. This difference in fracture length can primarily be attributed to the reduced propagation time within the hard core distribution region for low leakage coefficients [48]. The saved time allows the fracture to propagate more rapidly in the homogeneous reservoir after propagating through the hard core distribution region. Notably,, when the leakage coefficient decreases to 2.5×10^{-15} m/(mPa·s), the fracture propagation behavior in the stage beyond the hard-core distribution region differs markedly from that corresponding to higher leakage coefficients.. For this leakage coefficient, the fracture does not need to be redirected after propagating through the hard core distribution region, resulting in a rapid increase in fracture length. As shown in Figure 8(a), the final fracture length exceeds that of the conventional reservoir, reaching 48.05 m.

6 Conclusions and Future Work

The main conclusions are summarized as follows:

(1) The presence of hard cores in natural hydrogen reservoir can influence fracture propagation, but has a limited effect on fracture initiation behavior. For the hard-core-bearing model and the homogeneous model, the corresponding initiation pressures are 87.98 MPa and 87.87 MPa, respectively. There is almost no difference between the two. However, in models with hard cores, the fracture tends to widen while the length decreases. The final fracture length is reduced by 12.63% compared with that in the homogeneous reservoir, but the final width is increased by 18.49%.

(2) The presence of high-strength hard cores in reservoir can change the propagation path of fracture, resulting in "path optimization" (obstacle-avoidance) behavior. Therefore, within the hard core distribution region, fracture exhibits deflection followed by reorientation behavior, which will not be present

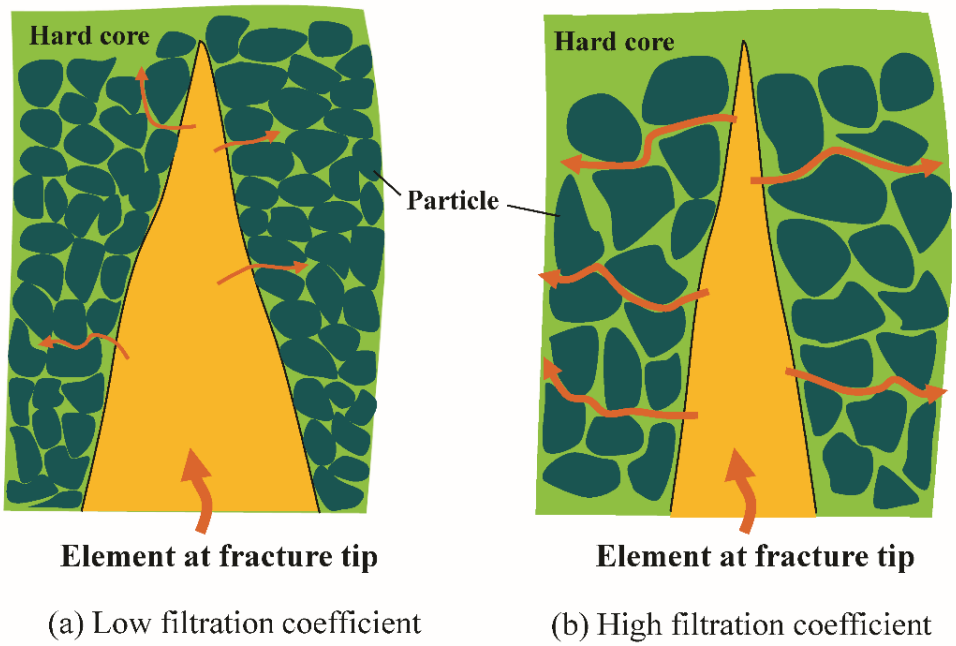

Figure 10. Comparison of the time taken for fracture propagating through three hard core elements under different leakage coefficients.

in the simulation with the homogeneous model. During fracture propagation and reorientation after propagating through the hard core distribution region, stress concentration around the fracture tip once again constrains its propagation.

(3) An increase in the tensile strength of hard cores restricts fracture propagation. Nevertheless, when the strength of hard core is not high, the fracture can still propagate through the hard core distribution region and continue to propagate. However, when the tensile strength exceeds a certain threshold, the hard cores will not fail, preventing fracture from propagating within them. Then, wide and short fracture formations in fracturing operation.

(4) Variations in the leakage coefficient can constrain fracture propagation by limiting the loss or leakage of working fluid through the fracture walls, then influencing fracture propagation. Its effect is mainly observed during the stage when the fracture propagates through the hard core distribution region. When the leakage coefficient decreases below a certain threshold, the fractures in the hard core distribution zone no longer exhibit deflection but instead propagate in a straight path.

Overall, this study provides a preliminary simulation-based understanding of natural hydrogen reservoir stimulation, while further comprehensive investigations are still necessary. Building upon the current findings, future research may focus on the following aspects:

(1) In subsequent simulation studies, geometric models incorporating soft cores and cavities can be developed to compare the differences in fracture behavior, and fracture morphology under the three types of imperfections.

(2) It should be noted that multi-cluster fracturing or interlayer interference effects have not been accounted in the current 2D model. In future work, 3D models can be developed to simulate the formation patterns of fracture networks under simultaneous initiation or zipper-like fracturing case, and to evaluate the effects of reservoir imperfections on fracture morphology, and connectivity.

(3) The effects of hard core strength and leakage coefficient have been analyzed in this study. In future investigations, additional variables such as injection rate, and in-situ stress differences, can be considered to quantify the respective influences. In addition, response surface methodology can be applied to optimize fracturing parameters.

Data Availability Statement

Data will be made available on request.

Funding

This work was supported without any funding.

Conflicts of Interest

Muhammad Usman Tahir is affiliated with the Atland Petro FZC, Sharjah 1377, United Arab Emirates, and Shenglan Guo is affiliated with the Guangzhou Gas Group Co., Ltd., Guangzhou 511436, China. The authors declare that these affiliations had no influence on the study design, data collection, analysis, interpretation, or the decision to publish, and that no other competing interests exist.

AI Use Statement

The authors declare that no generative AI was used in the preparation of this manuscript.

Ethical Approval and Consent to Participate

Not applicable.

References

[1] Zgonnik, V. (2020). The occurrence and geoscience of natural hydrogen: A comprehensive review. *Earth-Science Reviews, 203*, 103140. [CrossRef]

[2] Epelle, E. I., Obande, W., Udourioh, G. A., Afolabi, I. C., Desongu, K. S., Orivri, U., ... & Okolie, J. A. (2022). Perspectives and prospects of underground hydrogen storage and natural hydrogen. *Sustainable Energy & Fuels, 6*(14), 3324-3343. [CrossRef]

[3] Blay-Roger, R., Bach, W., Bobadilla, L. F., Reina, T. R., Odriozola, J. A., Amils, R., & Blay, V. (2024). Natural hydrogen in the energy transition: Fundamentals, promise, and enigmas. *Renewable and Sustainable Energy Reviews, 189*, 113888. [CrossRef]

[4] Qingchao, L., Jingjuan, W., Qiang, L., Fuling, W., & Yuanfang, C. (2025). Sediment Instability Caused by Gas Production from Hydrate-Bearing Sediment in Northern South China Sea by Horizontal Wellbore: Sensitivity Analysis. *Natural Resources Research*, 1-33. [CrossRef]

[5] Prinzhofer, A., Cissé, C. S. T., & Diallo, A. B. (2018). Discovery of a large accumulation of natural hydrogen in Bourakebougou (Mali). *International Journal of Hydrogen Energy, 43*(42), 19315-19326. [CrossRef]

[6] Fochesato, M., Peter, C., Morandi, L., & Lygeros, J. (2024). Peak shaving with hydrogen energy storage: From stochastic control to experiments on a 4 MWh facility. *Applied Energy, 376*, 123965. [CrossRef]

[7] Li, Q., Han, Y., Liu, X., Ansari, U., Cheng, Y., & Yan, C. (2022). Hydrate as a by-product in CO2 leakage during the long-term sub-seabed sequestration and its role in preventing further leakage. *Environmental Science and Pollution Research, 29*(51), 77737–77754. [CrossRef]

[8] Hassanpouryouzband, A., Armitage, T., Cowen, T., Thaysen, E. M., McMahon, S., Hajibeygi, H., ... & Haszeldine, R. S. (2025). The search for natural hydrogen: a hidden energy giant or an elusive dream?. *ACS Energy Letters, 10*(8), 3887-3891. [CrossRef]

[9] Arrouvel, C., & Prinzhofer, A. (2021). Genesis of natural hydrogen: New insights from thermodynamic simulations. *International Journal of Hydrogen Energy, 46*(36), 18780–18794. [CrossRef]

[10] Prinzhofer, A., Moretti, I., Françolin, J., Pacheco, C., d'Agostino, A., Werly, J., & Rupin, F. (2019). Natural hydrogen continuous emission from sedimentary basins: The example of a Brazilian H2-emitting structure. *International Journal of Hydrogen Energy, 44*(12), 5676-5685. [CrossRef]

[11] AlTammar, M. J., Agrawal, S., & Sharma, M. M. (2019). Effect of geological layer properties on hydraulic-fracture initiation and propagation: an experimental study. *SPE Journal, 24*(02), 757-794. [CrossRef]

[12] Deng, P., Ma, H., Song, J., Peng, X., Zhu, S., Xue, D., Jiang, L., & Chen, Z. (2025). Carbon dioxide as cushion gas for large-scale underground hydrogen storage: Mechanisms and implications. *Applied Energy, 388*, 125622. [CrossRef]

[13] Saeed, M., Jadhawar, P., & Bagala, S. (2023). Geochemical effects on storage gases and reservoir rock during underground hydrogen storage: A depleted North Sea oil reservoir case study. *Hydrogen, 4*(2), 323–337. [CrossRef]

[14] Ellis, G. S., & Gelman, S. E. (2024). Model predictions of global geologic hydrogen resources. *Science Advances, 10*(50), eado0955. [CrossRef]

[15] Dehghani, M. R., Ghazi, S. F., & Kazemzadeh, Y. (2024). Interfacial tension and wettability alteration during hydrogen and carbon dioxide storage in depleted gas reservoirs. *Scientific Reports, 14*(1), 11594. [CrossRef]

[16] Liu, K., Zhu, W., & Pan, B. (2024). Feasibility of hydrogen storage in depleted shale gas reservoir: A numerical investigation. *Fuel, 357*(Part B), 129703. [CrossRef]

[17] Muhammed, N. S., Haq, B., & Al Shehri, D. (2023). Role of methane as a cushion gas for hydrogen storage in depleted gas reservoirs. *International Journal of Hydrogen Energy, 48*(76), 29663–29681. [CrossRef]

[18] Guo, T., Wang, X., Li, Z., Gong, F., Lin, Q., Qu, Z., Lv, W., Tian, Q., & Xie, Z. (2019). Numerical simulation study on fracture propagation of zipper and synchronous fracturing in hydrogen energy development. *International Journal of Hydrogen Energy, 44*(11), 5270–5285. [CrossRef]

[19] Liang, X., Zhou, F., Liang, T., Wang, C., Wang, J., & Yuan, S. (2020). Impacts of low harm fracturing fluid on fossil hydrogen energy production in tight reservoirs. *International Journal of Hydrogen Energy, 45*(41), 21195–21204. [CrossRef]

[20] Liu, X., Qu, Z., Guo, T., Tian, Q., Lv, W., Xie,

Z., & Chu, C. (2019). An innovative technology of directional propagation of hydraulic fracture guided by radial holes in fossil hydrogen energy development. *International Journal of Hydrogen Energy, 44*(11), 5286–5302. [CrossRef]

[21] Lu, Y., Li, H., Lu, C., Wu, K., Chen, Z., Wang, K., Luo, H., & Shan, J. (2019). The effect of completion strategy on fracture propagation from multiple cluster perforations in fossil hydrogen energy development. *International Journal of Hydrogen Energy, 44*(14), 7168–7180. [CrossRef]

[22] Hosseini, S. I. M., Fahimpour, J., Ali, M., & Keshavarz, A. (2022). Capillary sealing efficiency analysis of caprocks: Implication for hydrogen geological storage. *Energy & Fuels, 36*(8), 4065–4075. [CrossRef]

[23] Yin, H., Yang, C., Ma, H., & Shi, X. (2020). Stability evaluation of underground gas storage salt caverns with micro-leakage interlayer in bedded rock salt of Jintan, China. *Acta Geotechnica, 15*(3), 549–563. [CrossRef]

[24] Shahmorad, Z., Salarirad, H., & Molladavoudi, H. (2016). A study on the effect of utilizing different constitutive models in the stability analysis of an underground gas storage within a salt structure. *Journal of Natural Gas Science and Engineering, 33*, 808–820. [CrossRef]

[25] Wang, L., Jin, Z., Liu, Q., Liu, K., Meng, Q., Huang, X., Su, Y., & Zhang, Q. (2024). The occurrence pattern of natural hydrogen in the Songliao Basin, PR China: Insights on natural hydrogen exploration. *International Journal of Hydrogen Energy, 50*(Part A), 261–275. [CrossRef]

[26] Lu, J., Muhammed, N. S., Okolie, J. A., & Epelle, E. I. (2025). A sensitivity study of hydrogen mixing with cushion gases for effective storage in porous media. *Sustainable Energy & Fuels, 9*(5), 1353–1370. [CrossRef]

[27] Hosseini, M., Ali, M., Fahimpour, J., Keshavarz, A., & Iglauer, S. (2022). Basalt-H2-brine wettability at geo-storage conditions: Implication for hydrogen storage in basaltic formations. *Journal of Energy Storage, 52*, 104745. [CrossRef]

[28] Li, Q., Li, Y., Cheng, Y., Li, Q., Wang, F., Wei, J., Liu, Y., Zhang, C., Song, B., Yan, C., & Ansari, U. (2018). Numerical simulation of fracture reorientation during hydraulic fracturing in perforated horizontal well in shale reservoirs. *Energy Sources, Part A: Recovery, Utilization, and Environmental Effects, 40*(15), 1807–1813. [CrossRef]

[29] Zamehrian, M., & Sedaee, B. (2022). Underground hydrogen storage in a naturally fractured gas reservoir: The role of fracture. *International Journal of Hydrogen Energy, 47*(93), 39606–39618. [CrossRef]

[30] Zeng, L., Sander, R., Chen, Y., & Xie, Q. (2024). Hydrogen storage performance during underground hydrogen storage in depleted gas reservoirs: A review. *Engineering, 40*, 211–225. [CrossRef]

[31] Ismail, A., & Azadbakht, S. (2024). A comprehensive review of numerical simulation methods for hydraulic fracturing. *International Journal for Numerical and Analytical Methods in Geomechanics, 48*(5), 1433–1459. [CrossRef]

[32] Ao, F., Qingchao, L., Qiang, L., Jingjuan, W., Fuling, W., & Chuanliang, Y. (2025). Numerical Simulation Investigation of Fracture Propagation Behavior Patterns and Sensitivity Factors of Oil Shale Reservoirs in the Xunyi Region Considering the Influence of Natural Fracture. *Geofluids, 2025*(1), 2762142. [CrossRef]

[33] Li, L. C., Tang, C. A., Li, G., Wang, S. Y., Liang, Z. Z., & Zhang, Y. B. (2012). Numerical simulation of 3D hydraulic fracturing based on an improved flow-stress-damage model and a parallel FEM technique. *Rock Mechanics and Rock Engineering, 45*(5), 801–818. [CrossRef]

[34] Hossain, M. M., & Rahman, M. K. (2008). Numerical simulation of complex fracture growth during tight reservoir stimulation by hydraulic fracturing. *Journal of Petroleum Science and Engineering, 60*(2), 86–104. [CrossRef]

[35] Li, D. Q., Zhang, S. C., & Zhang, S. A. (2014). Experimental and numerical simulation study on fracturing through interlayer to coal seam. *Journal of Natural Gas Science and Engineering, 21*, 386–396. [CrossRef]

[36] Zhao, Q., Lisjak, A., Mahabadi, O., Liu, Q., & Grasselli, G. (2014). Numerical simulation of hydraulic fracturing and associated microseismicity using finite-discrete element method. *Journal of Rock Mechanics and Geotechnical Engineering, 6*(6), 574–581. [CrossRef]

[37] Wang, T., Guo, Z., Li, G., Ma, Z., Yong, Y., & Tian, S. (2023). Numerical simulation of three-dimensional fracturing fracture propagation in radial wells. *Petroleum Exploration and Development, 50*(3), 699–711. [CrossRef]

[38] Guo, C., Xu, J., Wei, M., & Jiang, R. (2015). Experimental study and numerical simulation of hydraulic fracturing tight sandstone reservoirs. *Fuel, 159*, 334–344. [CrossRef]

[39] Xu, B., Liu, Y., Wang, Y., Yang, G., Yu, Q., & Wang, F. (2018). A new method and application of full 3D numerical simulation for hydraulic fracturing horizontal fracture. *Energies, 12*(1), 48. [CrossRef]

[40] Huang, L., Liao, X., Fan, M., Wu, S., Tan, P., & Yang, L. (2024). Experimental and numerical simulation technique for hydraulic fracturing of shale formations. *Advances in Geo-Energy Research, 13*(2), 83–88. [CrossRef]

[41] Sun, J., & Schechter, D. (2015). Investigating the effect of improved fracture conductivity on production performance of hydraulically fractured wells: Field-case studies and numerical simulations.

Journal of Canadian Petroleum Technology, 54(06), 442–449. [CrossRef]

[42] Ren, Q., Li, L., Wang, J., Jiang, R., Li, M., & Feng, J. (2024). Dynamic evolution mechanism of the fracturing fracture system—Enlightenments from hydraulic fracturing physical experiments and finite element numerical simulation. *Petroleum Science, 21*(6), 3839–3866. [CrossRef]

[43] Li, Y., Deng, J., Liu, W., Yan, W., Feng, Y., Cao, W., Wang, P., & Hou, Y. (2017). Numerical simulation of limited-entry multi-cluster fracturing in horizontal well. *Journal of Petroleum Science and Engineering, 152*, 443–455. [CrossRef]

[44] Zeng, Q., & Yao, J. (2016). Numerical simulation of fracture network generation in naturally fractured reservoirs. *Journal of Natural Gas Science and Engineering, 30*, 430–443. [CrossRef]

[45] Zhao, J., Wang, Z., Lin, R., Ren, L., Wu, J., & Wu, J. (2023). Numerical simulation of diverting fracturing for staged fracturing horizontal well in shale gas reservoir. *Journal of Energy Resources Technology, 145*(5), 053202. [CrossRef]

[46] Liu, X., Qu, Z., Guo, T., Sun, Y., Wang, Z., & Bakhshi, E. (2019). Numerical simulation of non-planar fracture propagation in multi-cluster fracturing with natural fractures based on Lattice methods. *Engineering Fracture Mechanics, 220*, 106625. [CrossRef]

[47] Lu, C., Ma, L., Li, Z., Huang, F., Huang, C., Yuan, H., & Guo, J. (2020). A novel hydraulic fracturing method based on the coupled CFD-DEM numerical simulation study. *Applied Sciences, 10*(9), 3027. [CrossRef]

[48] Sanchez, E. C. M., Cordero, J. A. R., & Roehl, D. (2020). Numerical simulation of three-dimensional fracture interaction. *Computers and Geotechnics, 122*, 103528. [CrossRef]

Muhammad Usman Tahir completed his MPhil at the University of the Punjab, Pakistan, at the age of 24, and is currently pursuing his PhD at the China University of Petroleum (East China) (Qingdao campus). His research focuses on investigating residual oil remobilization mechanisms using microfluidics and rock-on-a-chip techniques. His work aims to enhance oil recovery efficiency in mature fields through optimized simulation-based strategies such as water-alternating-gas (WAG) and chemical injection. By integrating technical and economic modeling, his study provides insights into maximizing hydrocarbon recovery and improving decision-making for sustainable oilfield development. (Email: uzain83@gmail.com)

Shenglan Guo completed his B.Eng at Chengdu University of Technology, China in 2016, and has obtained the M.Eng. at the School of Petroleum Engineering, China University of Petroleum (East China) in 2019. Her research focuses on the utilization of CO_2 in oil and gas development and the mechanisms of enhanced oil recovery (EOR). Her research seeks to improve reservoir modification efficiency and advance sustainable oil and gas development through the optimization of engineering simulation parameters. (Email: guosl2019@163.com)